SECTION-A

Intrinsic- Peroxidase Like Activity of Nanomaterials

5A.1. INTRODUCTION

In many physiological reactions Peroxidase enzyme based reactions has been extensively applied due to their high efficiency and specificity; however, they bear some intrinsic limitations such as low stability due to denaturation and digestion, dependency on environmental condition and expensive preparation as well as purification. These limitations have gained the researches attention to fabricate enzyme mimetic. Noble metal nanoparticles that mimic enzymes have become popular as they have potentiality for bio-signal amplification, due to their large surface area, high catalytic activity, and lowcost. Encouraged by multifunctional applications of inorganic nanomaterials, that mimic enzymes are very interesting as they have better properties comparing to natural enzymes like more resistance to pH, temperature, protease digestion, large surface area, and high catalytic activity, lowcost, easier to prepare and store. Recently, it has been reported that many nanomaterials could have intrinsic peroxidase like activity, justifying their use as peroxidase substitute for health and health care advances [Bhattacharya *et al.*, (2011); Chen *et al.*, (2013); Liu *et al.*, (2012); Ma *et al.*, (2012); Malvi *et al.*, (2012); Wang *et al.*, (2012); Wei and Wang, (2013); Yu *et al.*, (2009); Zhang *et al.*, (2012); Qiao *et al.*, (2014); Deng *et al.*, (2014)]. This intended us to study the following: (1) to understand the compatibility of AgNPs and Au-Ag BMNPs for evaluation their role in biocatalysis, and (2) to evaluate the possibility on the formation of nanocomposite consisting of the matrix material containing the nanosized reinforcement components facilitating the electron transfer and catalytic performances of nanocomposite.

In particular, AgNPs, Au-Ag BMNPs and PBNPs based nanocomposites attract special research interest illustrate admirable electrochemical properties for potential applications and in addition to that the intrinsic peroxidase-like activity for the nanomaterials. Fortunately, we got interesting finding on these line that led to examine further on the peroxidase mimetic and electrochemical behavior of the

nanocomposite toward detection of H_2O_2. The findings revealed that electrocatalysis is greatly amplified due to incorporation of AgNPs into the matrix of PBNPs.

5A.2. EXPERIMENTAL

5A.2.1. Materials

The following chemicals were used: *o*-dianisidine obtained from Sigma-Aldrich Chem. Co. India; hydrogen peroxide obtained from Merck, India. All other chemicals employed were of analytical grade. PdNPs and nanocomposite of PBNPs with AgNPs/ Au-Ag were synthesized in the Chapter 3 and 4. Aqueous solutions were prepared by using doubly distilled-deionized water (Alga water purification system). The solutions of H_2O_2 were freshly prepared in double distilled water before each experiment.

5A.2.2. Peroxidase-like catalytic activity of PBNP-AgNPs/PBNP-Au-Ag

The peroxidase like activity of as synthesized nanocomposite (as discussed in section 4.2.2.3) was determined spectrophotometrically by measuring the formation of the oxidized product of *o*-dianisidine at 430 nm respectively, using a Hitachi U-2900 spectrophotometer. In general, the *o*-dianisidine oxidation activity was measured in 0.1 M phosphate buffer (pH 7.0) in the presence of nanocomposite (20 µL mL^{-1}) using 60 µM *o*-dianisidine during 300 s at 25^oC. H_2O_2 (1 mM) was added to start the reaction, unless otherwise specified.

5A.2.3. Peroxidase-like catalytic activity of PdNPs

The peroxidase like activity of as synthesized palladium nanoparticles (PdNPs) was determined spectrophotometrically by measuring the formation of the oxidized product of *o*-dianisidine at 430 nm respectively, using a Hitachi U-2900 spectrophotometer. In general, the *o*-dianisidine oxidation activity was measured in 0.1 M phosphate buffer (pH 7.0) in the presence of PdNPs (30 µL mL^{-1}) using 60 µM o-dianisidine during 50 s at 25^oC. PdNPs made at four compositions (as discussed in Chapter 3, Table 3.2: $PdNP_1$, $PdNP_2$, $PdNP_3$ and $PdNP_4$) Hydrogen peroxide (1 mM) was added to start the reaction, unless otherwise specified.

5A.2.4. Kinetic Parameter Analysis

Steady-state kinetics was performed in the case of Nanocomposite (PBNP-AgNP/PBNP-Au-Ag) by varying the concentration of H_2O_2 (0-50 mM), or *o*-dianisidine (0-0.68 mM) at a fixed concentration of *o*-dianisidine or H_2O_2. The reaction was carried out in 2 mL phosphate buffer (0.1 M, pH 7.0) and the variation of the absorbance was monitored using a spectrophotometer (Hitachi U-2900) in the time scan mode at 430 nm (ε=11.3 $mM^{-1}cm^{-1}$). The kinetic parameters were calculated by fitting the absorbance data to the Michaelis-Menten equation as,

$$\nu = V_{max}[C]/K_m + [C]$$

Where ν is the initial velocity, V_{max} is the maximal reaction velocity, C is the concentration of the substrate, and K_m is the Michaelis-Menten constant.

Further steady-state kinetics was performed in the case of PdNPs by varying the concentration of H_2O_2 (0-50 mM), at a fixed concentration of *o*-dianisidine.

5A.3. RESULTS

5A.3.1. Peroxidase-like activities of PBNPs-AgNPs/Au-Ag nanoparticles

Since PBNPs represent an excellent class of peroxidase mimetics, the PBNP nanocomposite may be a suitable candidate for peroxidase replacement. First stage of investigation is to authenticate the peroxidase mimetic activity of nanocomposite of PBNP with monometallic as well as bimetallic nanoparticles; as a result, we examined the findings of these issues through the catalytic oxidation of peroxidase substrate *o*-dianisidine, in the presence of H_2O_2 (Scheme 5A.1). Figure 5A.1 shows the visual photographs of nanocomposite catalyzed oxidized product of *o*-dianisidine producing an orange brown colour. In order to have deeper insight on the kinetic analysis, UV-Vis spectra of the reaction system and spectral change as function of substrate concentrations was studied.

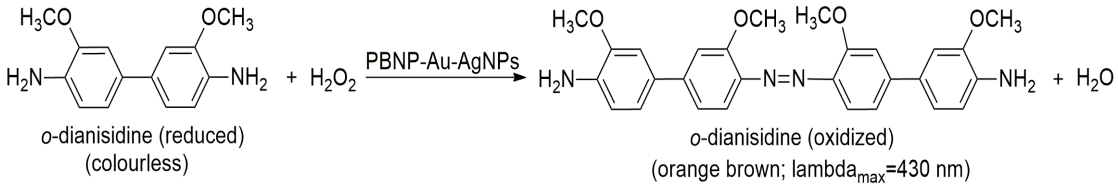

Scheme 5A.1. The reaction scheme of oxidation of *o*-dianisidine.

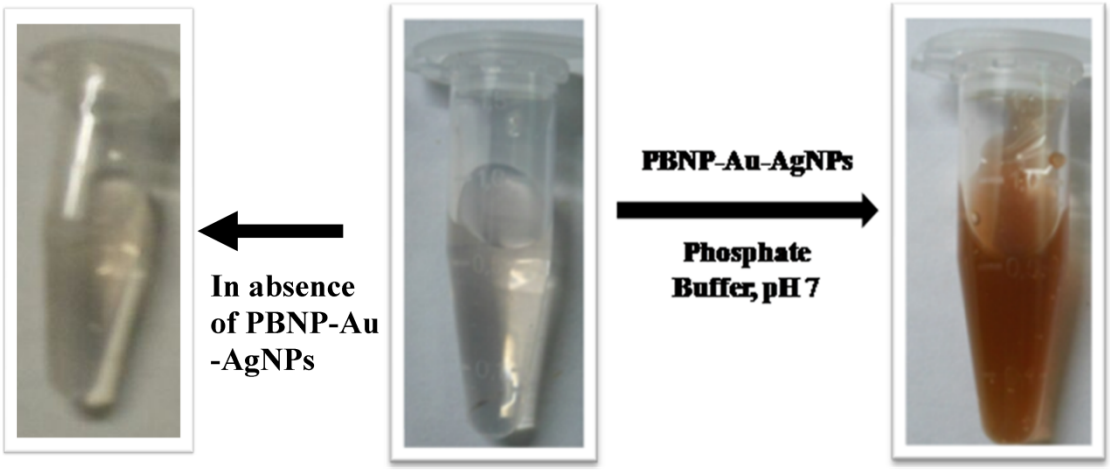

Figure.5A.1. Photographs showing the production of coloured product in the presence and absence of PBNP-Au-AgNPs to *o*-dianisidine in phosphate buffer pH (7.0)

5A.3.2. Steady-state kinetic analysis

5A.3.2.1. Oxidation of Peroxidase substrate o-dianisidine

The UV-Vis spectra of the reaction system containing *o*-dianisidine, H_2O_2 and nanocomposite of PBNP with Au-Ag nanoparticles are shown in Figure 5A.2. The results were recorded for 6 consecutive cycles and revealed an increase of absorbance at 430 nm corresponding to the oxidized product of *o*-dianisidine. To investigate the apparent steady-state reaction rates, time-scan was started as quickly as possible and the absorbance variation with time was continuously monitored at 430 nm. The kinetic parameters of PBNP-Au-Ag for the reactions were evaluated by the initial rate method. The absorbance data were converted to corresponding concentration terms by using the value $\varepsilon = 11.3\ mM^{-1}\ cm^{-1}$ (at 430 nm) for the oxidized product of *o*-dianisidine.

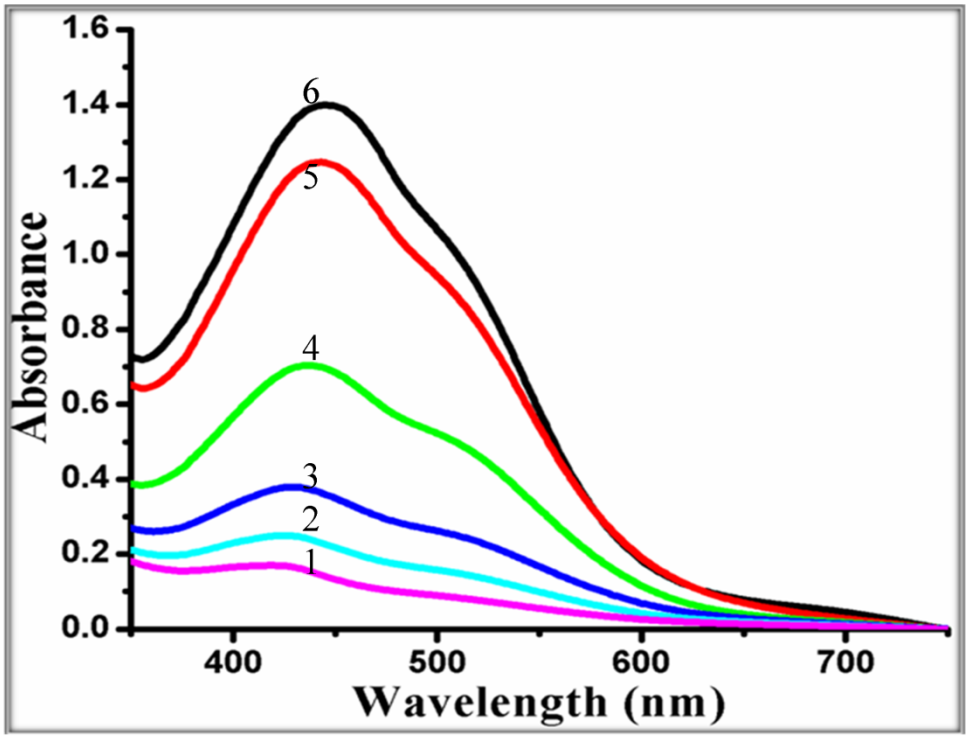

Figure. 5A.2. Typical UV-Vis spectra of *o*-dianisidine-H_2O_2-PBNP-Au-AgNP reaction system at different concentration of H_2O_2 (1-0.1, 2-0.4, 3-1.61, 4-6.46, 5-25.84, 6-51.67×10^{-3} M) recorded after 3 minutes from the addition of catalyst.

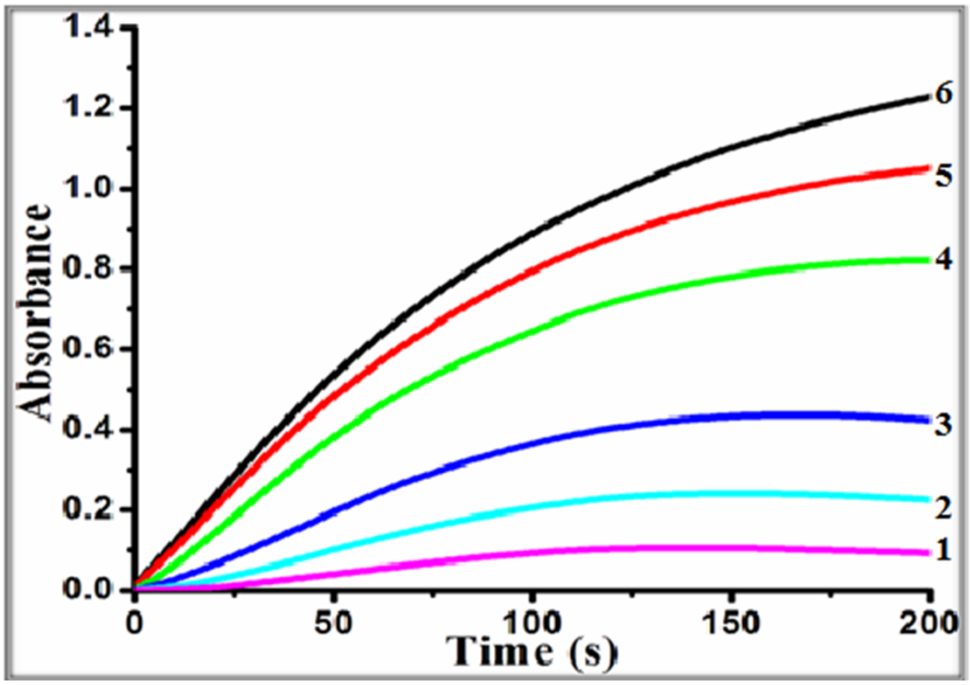

Figure. 5A.3. Time-dependent absorbance changes at 430 nm in the presence of PBNP-Au-AgNP nanoparticles at different concentration of H_2O_2 (1-0.1, 2-0.4, 3-1.61, 4-6.46, 5-25.84, 6-51.67×10^{-3} M).

5A.3.3. Peroxidase mimetic efficiency of PdNPs made through Cyclohexanone

PdNPs made through Cyclohexanone, due to sufficient stability, biocompatibility and possibility of its synthesis at the time of application make a potential candidate of peroxidase mimetic. Accordingly, attempt has been made to evaluate the peroxidase mimetic ability of as-synthesized PdNPs as a function of 3-APTMS and cyclohexanone concentrations towards the oxidation of *o*-dianisidine. Since, the catalytic activity of PdNPs is H_2O_2 concentration-dependent, this can be used to detect H_2O_2. Figure 5A.4 shows the visual photographs of PdNPs catalyzed oxidized product of *o*-dianisidine at various concentration of H_2O_2 from 1 to 9 (0.1, 0.2, 0.4, 0.8, 1.61, 3.23, 6.46, 25.84, 51.67x10^{-3} M) producing an orange brown colour. The results on the absorbance vs wavelength in the presence of different concentration of H_2O_2 as shown in Figure 5A.4 and fixed concentration of *o*-dianisidine catalyzed by PdNPs ($PdNP_1$, $PdNP_2$, $PdNP_3$ and $PdNP_4$) are shown in Figure 5A.5-8 revealed that the reaction catalyzed by PdNPs displayed Michaelis-Menten kinetics.

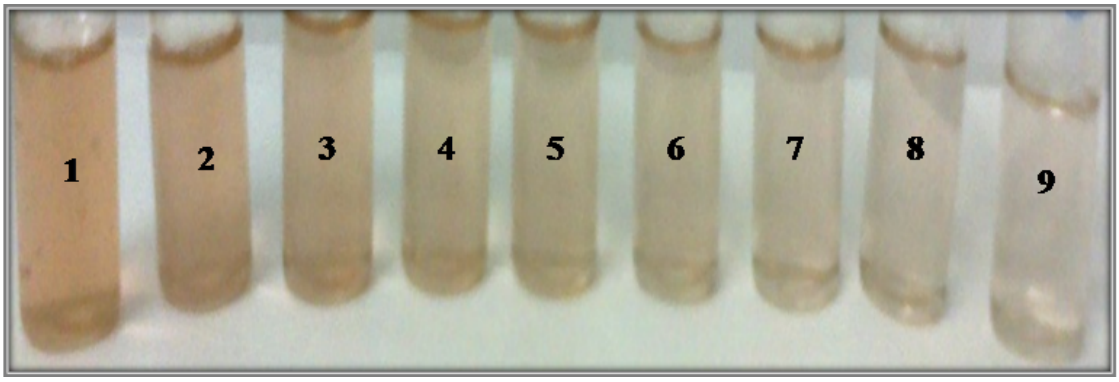

Figure 5A.4. The photographs showing colour evaluation upon addition of *o*-dianisidine by varying concentrations of H_2O_2 and constant PdNPs.

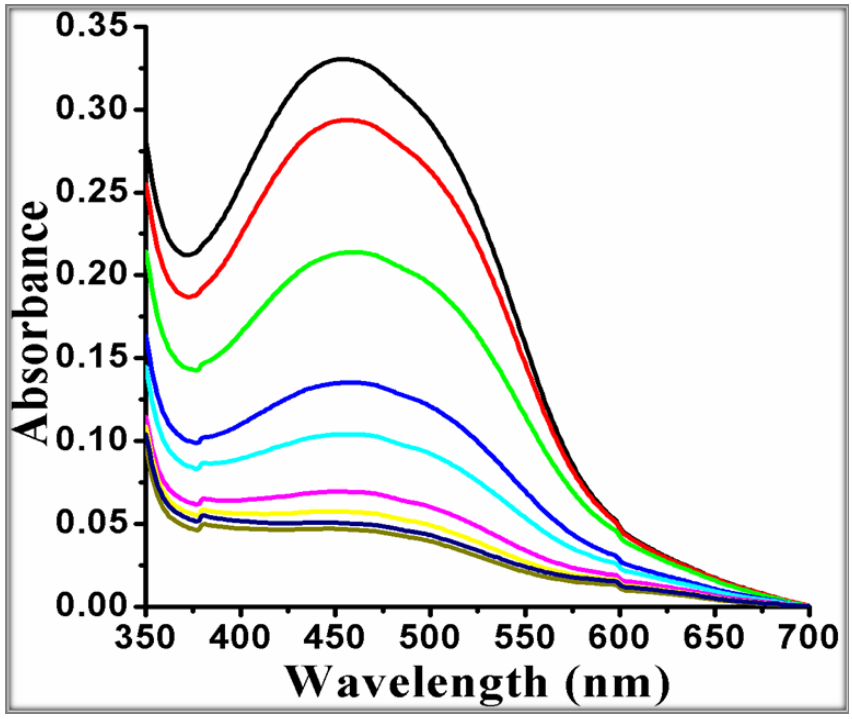

Figure. 5A.5. Represent the UV-Vis spectra of *o*-dianisidine oxidation products on the addition of $PdNP_1$ with various concentrations of H_2O_2 (0.1, 0.2, 0.4, 0.8, 1.61, 3.23, 6.46, 25.84, 51.67x 10^{-3} M).

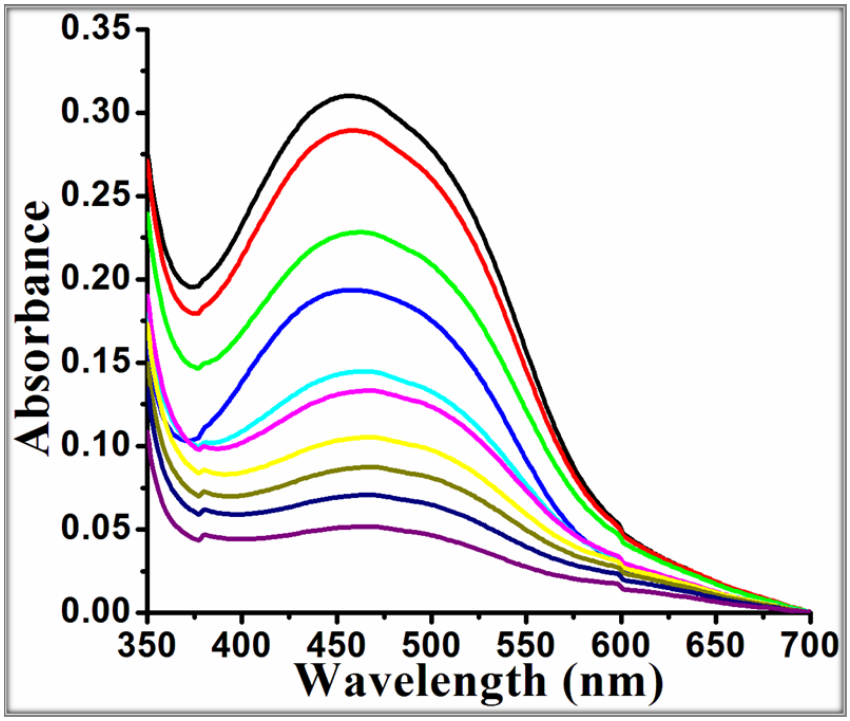

Figure 5A.6. Represent the UV-vis spectra of *o*-dianisidine oxidation products on the addition of $PdNP_2$ with various concentrations of H_2O_2 (0.1, 0.2, 0.4, 0.8, 1.61, 3.23, 6.46, 25.84, 51.67x 10^{-3} M).

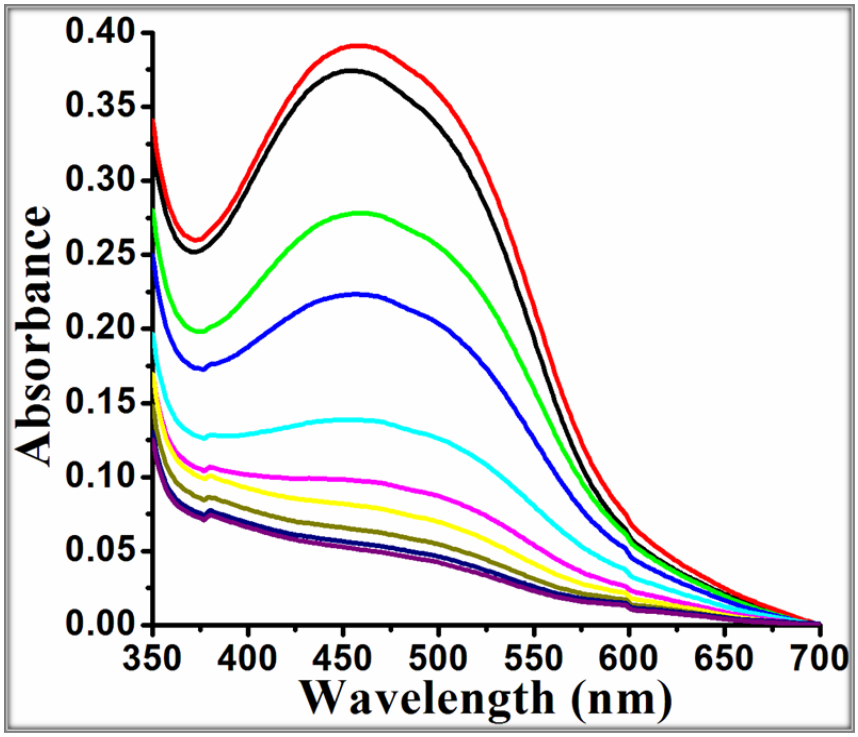

Figure 5A.7. Represent the UV-vis spectra of *o*-dianisidine oxidation products on the addition of $PdNP_3$ with various concentrations of H_2O_2 (0.1, 0.2, 0.4, 0.8, 1.61, 3.23, 6.46, 25.84, 51.67x 10^{-3} M).

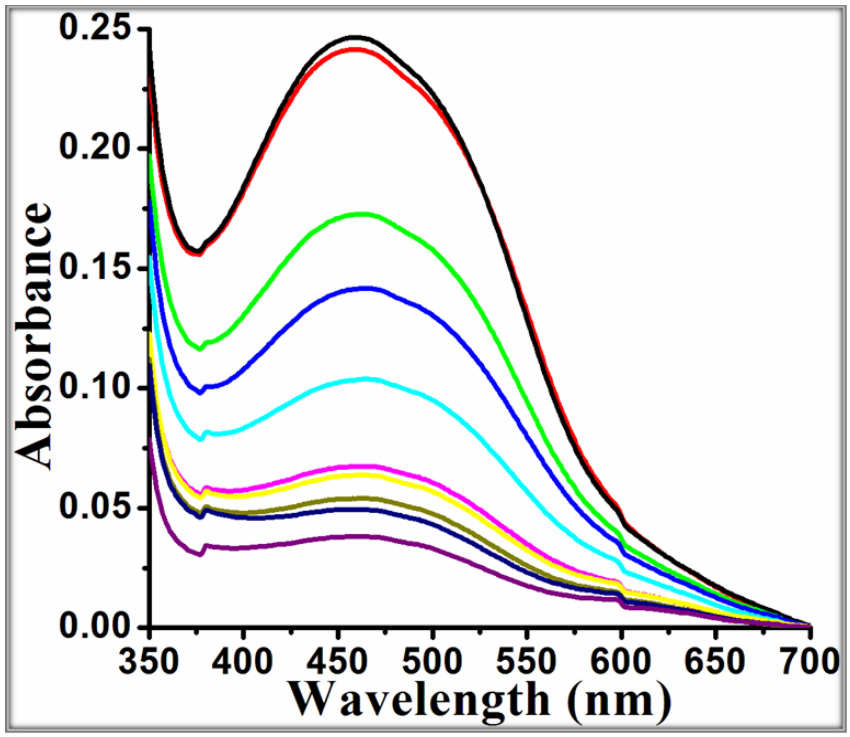

Figure 5A.8. Represent the UV-vis spectra of o-dianisidine oxidation products on the addition of $PdNP_4$ with various concentrations of H_2O_2 (0.1, 0.2, 0.4, 0.8, 1.61, 3.23, 6.46, 25.84, 51.67x 10^{-3} M).

5A.4. DISCUSSION

5A.4.1. Nanocomposite of PBNPs-AgNPs/Au-Ag catalyse the oxidation of peroxidase substrate- *o*-dianisidine

Generally, peroxidase enzyme, H_2O_2 and color substrate based systems are typically employed for routine applications in ELISA kits and other bioassay. The catalytic mechanism involves the enzyme catalysis of the two electron reduction of H_2O_2 to H_2O to form an intermediate complex; the colour substrate binds to the complex by a nucleophilic attack, thus allowing the oxidation reaction to occur with a colour change. The activity of peroxidase in such kit remains in question due to least stability of the same for practical applications. These disadvantages have directed for investigating enzyme mimetics. Accordingly, the requirement for an HRP-mimetic has been an important area of research. Recently, it has been reported that many nanomaterials, such as noble metal nanoparticles, metal oxide, Prussian blue and their composites possess intrinsic peroxidase-like activity and have proclaimed their use as peroxidase replacement. In this chapter, we provide the finding on the mimetic ability of Nanocomposite of PBNPs-AgNPs/Au-Ag using *o*-dianisidine as peroxidase substrate.

To investigate the enzyme mimetic activity of the Nanocomposite of PBNPs-AgNPs/Au-Ag, first, the catalytic experiments were carried out using *o*-dianisidine as substrate. As can be inferred from Figure 5A.1 and 5A.2, the colourless *o*-dianisidine forms a brown product when allowed to react with H_2O_2 and PBNPs-AgNPs/Au-Ag and the resulting colour change can be read on a spectrophotometer at a wavelength of 430 nm. The mimetic reaction was further proven by Michaelis-Menten curves. Typical Michaelis-Menten curves can be obtained for the nanodispersion of PBNPs-AgNPs/Au-Ag with both H_2O_2 and *o*-dianisidine as substrates shown in Figure 5A.9 and Michaelis-Menten curve for the nanodispersion of PBNPs-$AgNP_1$, PBNP-$AgNP_4$ and PBNP-$AgNP_5$ with H_2O_2 as substrate shown in Figure 5A.10-11. The enzyme kinetic parameters such as [Michaelis constant (K_m) and maximum initial velocity (V_{max})] were obtained in Table 5A.1. Table 5A.1 compared the K_m and V_{max} values of PBNP-Au-Ag, PBNP-$AgNP_1$, PBNP-$AgNP_4$, PBNP-$AgNP_5$, PBNP and HRP. K_m is

an indicator of enzyme affinity for its substrate. A high K_m value indicates weaker affinity, whereas a low value suggests a higher affinity. The results justify the better catalytic behaviour of PBNP-Au-Ag as compared with PBNP-$AgNP_4$, PBNP-$AgNP_5$, PBNP-$AgNP_1$ and PBNP. The apparent K_m value of Nanocomposite of PBNPs-AgNPs/Au-Ag was compared with HRP, which confirmed that PBNP-Au-Ag shows significantly enhanced kinetic catalytic behavior as compared to that of HRP (Table 5A.1.). The apparent K_m value of PBNP-Au-Ag with H_2O_2 as the substrate was found to be 1.7 mM whereas it was 3.7 mM for HRP under the present experimental conditions. The operation stability of all the Nanocomposite of PBNPs-AgNPs/Au-Ag in the physiological pH range are significantly longer for practical application accordingly the Nanocomposite of PBNPs-AgNPs/Au-Ag behave as perfect peroxidase replacements with super peroxidase activity for technological development. Our findings further revealed that the catalytic behavior of PBNP-Au-Ag was remarkably better than that of HRP as fast catalysis within minutes of the oxidation of o-dianisidine in the absence of H_2O_2 was recorded, which was judged by the appearance of the characteristic colour in phosphate buffer solutions (pH 7.0) and by the corresponding UV-Vis spectrum.

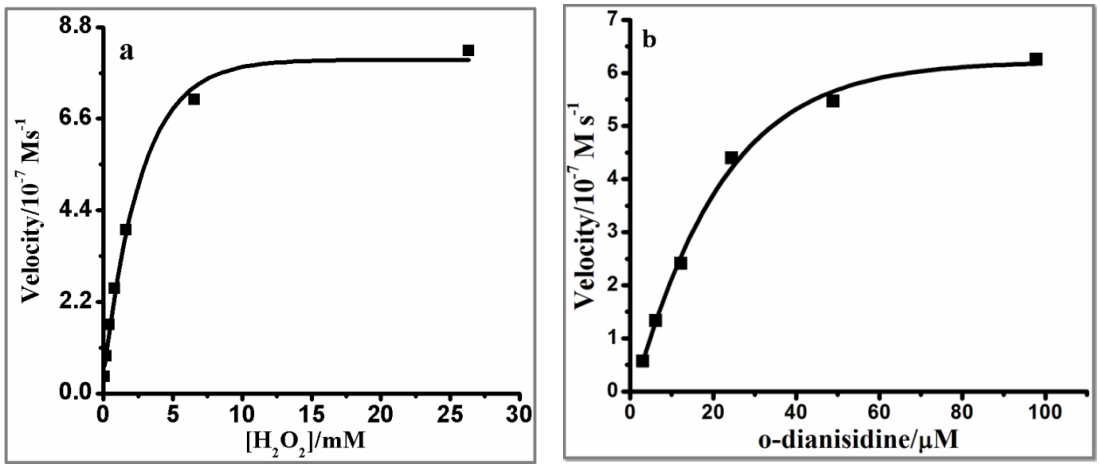

Figure 5A.9. (a) Kinetic analysis of PBNP-Au-Ag with H_2O_2 as substrate; and **(b)** kinetic analysis of *o*-dianisidine as substrate.

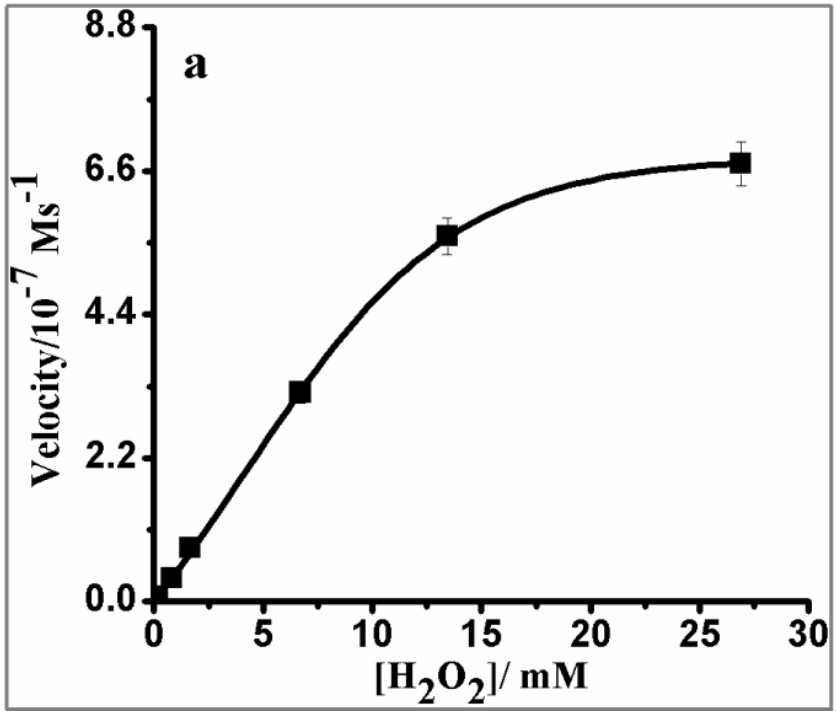

Figure 5A.10. Kinetic analysis of PBNP-AgNP$_1$ with H_2O_2 as substrate.

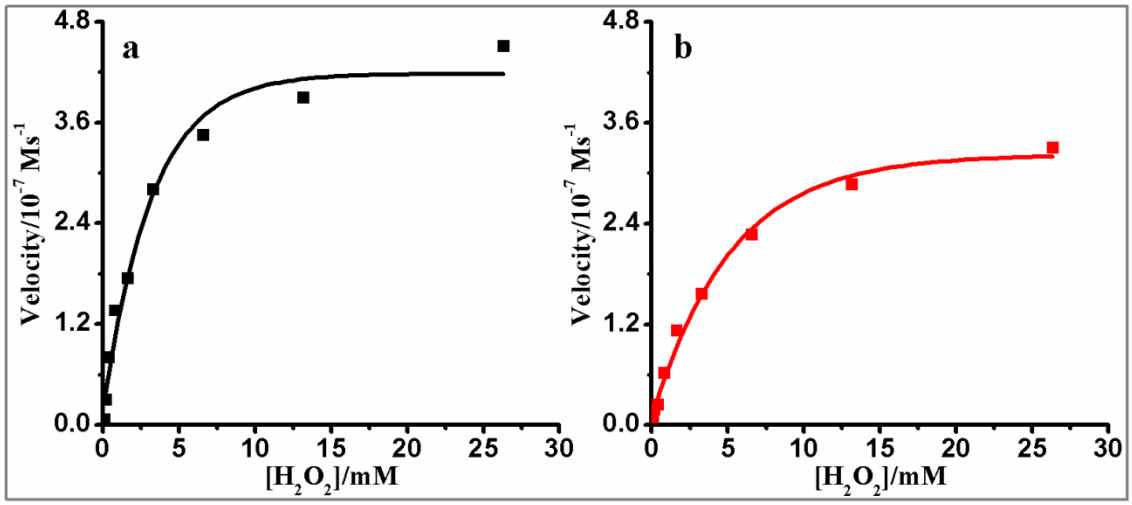

Figure 5A.11. (a) Kinetic analysis of PBNP-AgNP$_5$ and **(b)** PBNP-AgNP$_4$ with H_2O_2 as substrate.

Table 5A.1. Kinetic parameters for the peroxidase-like activity of PBNP-AgNPs and PBNP-Au-Ag nanocomposite

S.No.	Catalyst	Substrate	K_m/mM	V_{max}/ms^{-1}
1	PBNP	H_2O_2	9.04	8.40 x 10^{-7}
2	PBNP-$AgNP_4$	H_2O_2	3.32	3.15 x 10^{-7}
3	PBNP-$AgNP_5$	H_2O_2	2.05	4.15 x 10^{-7}
4	PBNP-Au-Ag	H_2O_2 o-dianisidine	1.7 0.015	7.82 x 10^{-7} 5.75x10^{-7}
5	PBNP-$AgNP_1$	H_2O_2	6.6	6.30 x 10^{-7}
6	HRP^{ref}	H_2O_2	3.7	8.71 x 10^{-7}

Ref-[Gao *et al.*, (2007), Zhang *et al.*, (2010)]

5A.4.2. Nanoparticles of Palladium catalyse the oxidation of *o*-dianisidine

As-synthesized PdNPs make a potential candidate of peroxidase mimetic. Typical Michaelis-Menten curves can be obtained for the PdNPs ($PdNP_1$, $PdNP_2$, $PdNP_3$ and $PdNP_4$) shown in Figure 5A.12-13 made with increasing concentrations of 3-APTMS and cyclohexanone on the oxidation of *o*-dianisidine-H_2O_2 system. The K_m value of PdNPs increases with increase in 3-APTMS concentrations as shown in Table 5A.2. At lower concentration of 3-APTMS and cyclohexanone, K_m value is found close to 3.6 mM. Such a low K_m value recorded using feasible amount of PdNPs when compared with HRP catalyzed reaction (3.7 mM) involving possible amount of active protein to exploit during routine laboratory direct the use of as synthesized nanoparticles in technological evolution.

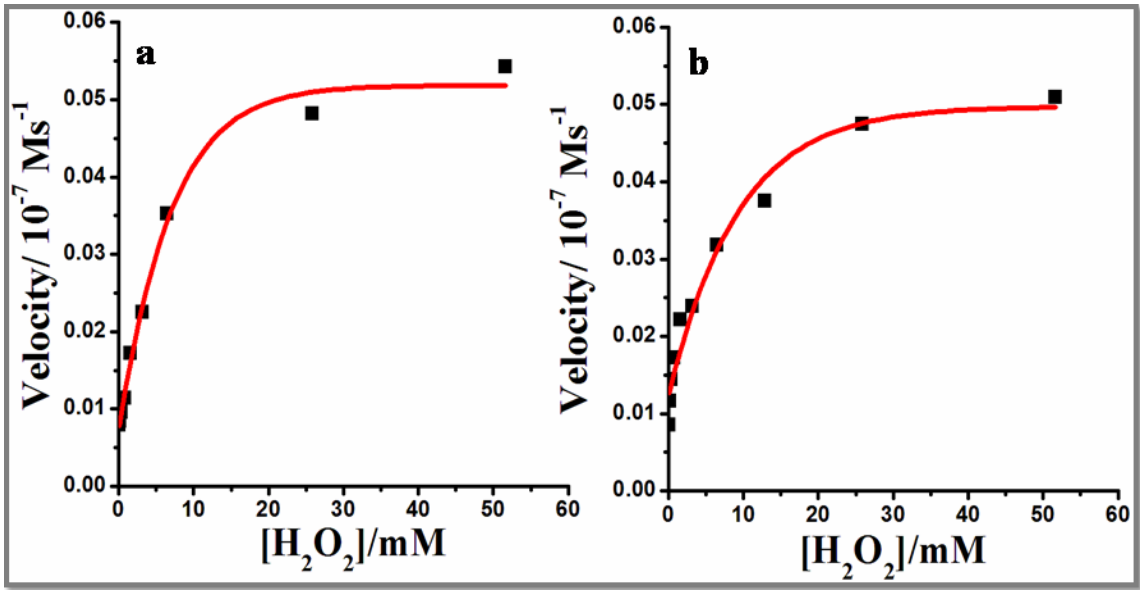

Figure 5A.12. Steady-state kinetic assay of $PdNP_1$ (a) and $PdNP_2$ (b).

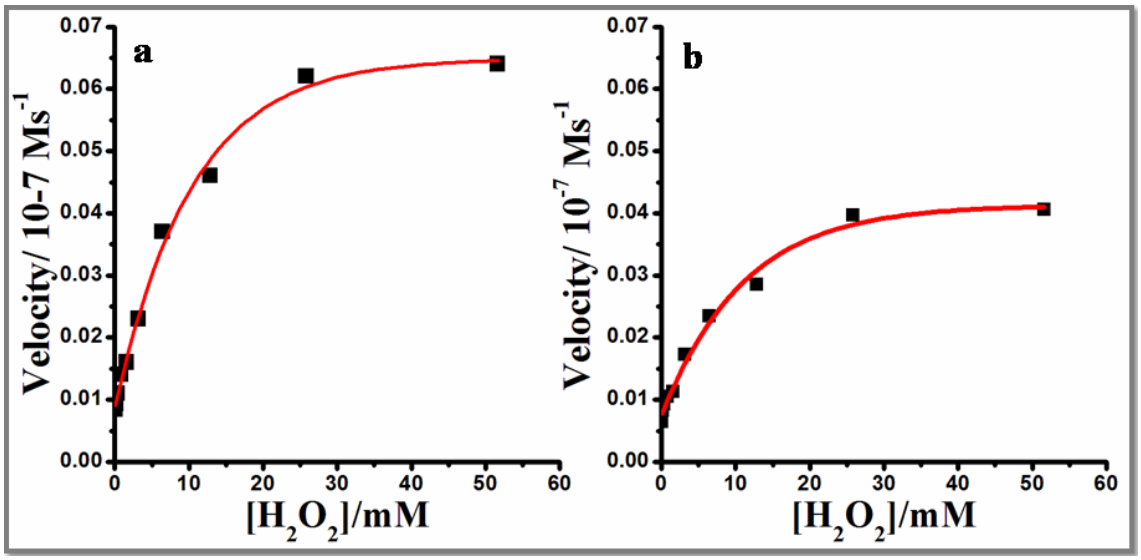

Figure 5A.13. Steady-state kinetic assay of $PdNP_3$ (a) and $PdNP_4$ (b).

Table 5A.2. Kinetic parameters for the peroxidase-like activity of PdNPs

S.No.	Catalyst	Substrate	K_m/mM	V_{max}/ms^{-1}
1	$PdNP_1$	H_2O_2	3.6	0.051×10^{-7}
2	$PdNP_2$	H_2O_2	4.0	0.049×10^{-7}
3	$PdNP_3$	H_2O_2	4.8	0.064×10^{-7}
4	$PdNP_4$	H_2O_2	5.3	0.041×10^{-7}

5A.5. CONCLUSION

Herein, we investigated that PBNP-AgNP and PBNP-Au-AgNP possess intrinsic peroxidase like activity capable of catalyzing the oxidation of typical substrate *o*-dianisidine, by H_2O_2. The results based on these lines reveals the following: (i) the PBNP-Au-AgNP nanocomposite show an enhanced catalytic efficiency as compared to that of PBNPs and PBNP-AgNP made under similar conditions; (ii) The relative variation in the kinetic catalytic activity of PBNP-AgNP and PBNP-Au-AgNP was examined for H_2O_2 detection and found in the order of: PBNP-Au-AgNP > PBNP-$AgNP_5$ > PBNP-$AgNP_4$ > PBNP-$AgNP_1$ > PBNPs and (iii) The results justified the better kinetic catalytic behavior of PBNP-Au-AgNP as compared to that of PBNPs and PBNP-AgNP revealed the bimetallic nanocomposite is more catalytic than monometallic nanocomposite as well as PBNPs; Further, the as generated palladium nanoparticles show excellent intrinsic peroxidase like activity with K_m value to the order of 3.6 mM indicating complete replacement of HRP used in biomedical application. Some other major findings of this chapter is as follows: (i) the catalytic property of PdNPs made with increasing concentrations of 3-APTMS and cyclohexanone on the oxidation of *o*-dianisidine-H_2O_2 system; (ii) the K_m value of PdNPs increases with increase in 3-APTMSconcentrations; and (iii) the relative variation in the kinetic catalytic activity of PdNPs was examined for H_2O_2 detection and found in the order of: $PdNP_1$>$PdNP_2$>$PdNP_3$> $PdNP_4$.

SECTION-B

Electrocatalytic Activity of Nanomaterials

5B.1. INTRODUCTION

Extensive reports on the use of ferrocene and its derivatives as electron transfer mediator are documented during last three decades, justifying the commercial design of electrochemical biosensors [Cass *et al*., (1984); Amine *et al*., (1991); Cash *et al*., (2010); Takahashi *et al*., (2013)]. The pioneering work of Hill *et al* demonstrated the mechanism of mediated electron transfer from redox biomolecule in homogeneous system [Cass *et al*., (1984)]. Since the practical application of such material normally involves heterogeneous system. Carbon paste has been one of most conventional microporous matrix allow efficient mediation between redox centre of biomolecule and electron transfer mediator [Pandey *et al*., (1998); Pandey *et al*., (1992); Pandey *et al*., (1993); Pandey., (Patent-1995); Beitollahi *et al*., (2011); Beitollahi *et al*., (1940)].

However, micro-porosity of the same restrict efficient utilization on the mediator for bioelectrochemical sensing in reliable practical design attributed to the leaching out of the same from the matrix. Such limitation of microporous matrices directed our attention to understand the practical utility of ferrocene derivatives when incorporated within nanostructured network of organically modified silicate (ORMOSIL) film. Such film could be made from the use of functional alkoxysilanes through sol-gel process having most suitable option for encapsulating the small molecules like ferrocene [Pandey *et al*., (1999e);]. Nanostructured matrix formation takes place by controlling the hydrophobic and hydrophilic components of alkoxysilane precursors such as 3-glycidoxypropyltrimethoxysilane (GPTMS), 2- (3-epoxycyclohexyl) ethyltrimethoxysilane (ECETMS), 3-aminopropyltrimethoxysilane (3-APTMS) and trimethoxysilane (TMS). There is the two combinations of hydrophobic and hydrophilic components e.g. (1) GPTMS andTMS; (2) 3-APTMS and ECETMS; in appropriate ratio were used for encapsulating the ferrocene monocarboxylic acid (Fc-COOH). The redox electrochemistry of Fc-COOH in both

cases was found to display sluggish reversible electrochemistry due to restricted mobility of ferrocenium ions within nanostructured domain. These findings directed us to design ormosil film fulfilling the requirement of ferrocene-mediated bioelectrochemical sensing and there is the choice of electrocatalyst in combination with encapsulated mediator for facilitating electron transfer process. Fortunately the interaction of palladium chloride/tetrachlorpalladate ($PdCl_2/K_2PdCl_4$) was found, in which palladium ions opens the epoxide ring of glycidoxy residue and in turn gets reduced into palladium followed by subsequent co-ordination within two glycidoxy residue [Pandey *et al.*, (2001c); Pandey *et al.*, (2003d)].

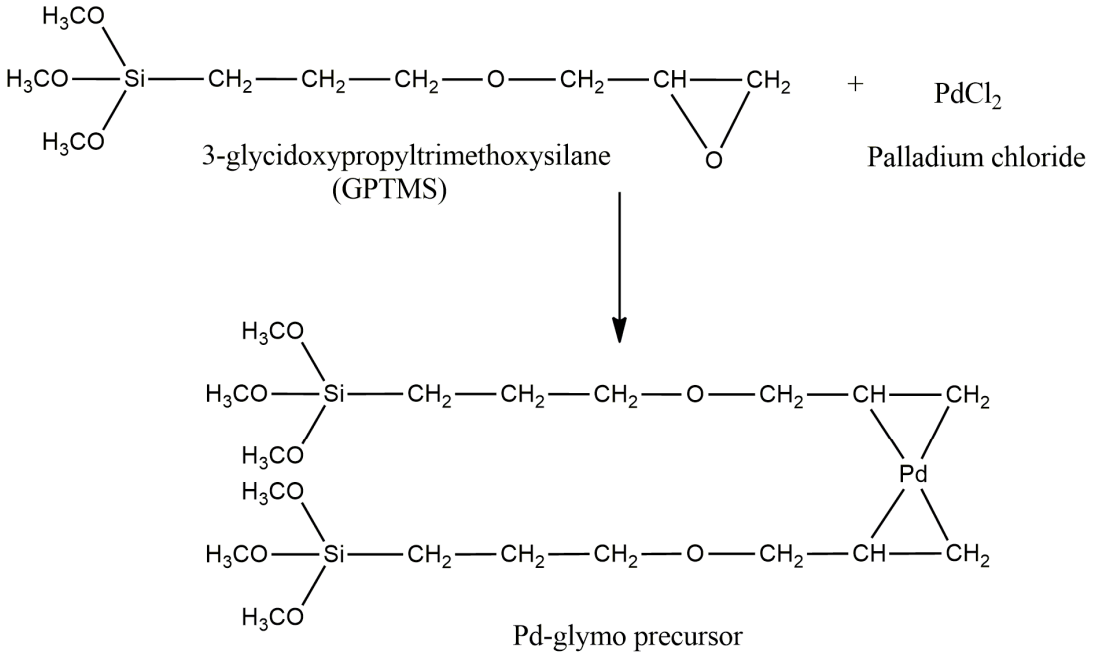

Scheme 5B.1 Specific interaction in between GPTMS and $PdCl_2$

The redox electrochemistry of the Fc-COOH within ormosil film made from palladium linked-GPTMS and TMS showed excellent reversible electrochemistry even better than that of the same recorded in homogeneous solution [Pandey *et al.*, (2001c)]. The reasons for excellent reversible redox electrochemical behavior of ferrocene in such system, we found that trimethoxysilane (TMS) itself interact with $PdCl_2$ and results into the formation of Pd-Si linkage [Pandey *et al.*, (2001c); Pandey and Upadhyay., (2005a)] and enable the formation of novel nanostructured domains in the presence of palladium-linked GPTMS justifying as solid solution matrix for

practical application of material in technological design. It has been found that ECETMS also undergo interaction with $PdCl_2$ through epoxide ring of cyclohexyl group of alkoxysilane [Pandey *et al.*, (2001c)] however, enable the dissociation of organic functionality and affect the water wettability of the ormosil film that alter the electrochemical behavior of ferrocene within ormosil network. In addition to that the role of 3-APTMS influencing the electrochemical behavior of ferrocene derivative. Such requirement directed our attention to understand the role of palladium nanoparticles (PdNPs) of known nanogeometry on the redox behavior of Fc-COOH in the presence and absence of 3-APTMS since, redox electrochemistry of the same is influenced in the presence of metal nanoparticles [Kusamoto *et al.*, (2009)]. Recently, we have demonstrated that 3-APTMS acts as an active reagent for the synthesis and stabilization of NMNPs of palladium, gold and silver [Pandey and Chauhan., (2012); Pandey *et al*; (2014a); Pandey and Pandey., (2014c); Pandey *et al*; (2014b)]. Further, the use of 3-APTMS, tetrahydrofuronhydroperoxide (THF-HPO) has been investigated and the findings justify precise conversion of Au^{3+} into gold nanoparticles (AuNPs) [Pandey and Pandey., (2014c)] and conversion of palladium salt into PdNPs (as discussed in Chapter 3). These PdNPs may again used for investigating their role on reversible redox electrochemistry of Fc-COOH. Accordingly, in present chapter for investigating the followings; (1) interaction of 3-APTMS and Fc-COOH if any, (2) effect of nanostructured palladium of variable nanogeometry on the electrochemistry of Fc-COOH and (3) to understand the electrocatalysis of nanostructured palladium and Fc-COOH modified electrodes. The finding on the role of PdNPs for versatile applications has been investigated and reported in this chapter.

5B.2. EXPERIMENTAL

5B.2.1. Materials and Instrumentation

The following chemicals were used: Ferrocenemonocarboxylic acid (Fc-COOH), Graphite powder (particle size 1-2 μm), Nujol oil (density 0.838 g mL^{-1}). Electrochemical experiments were performed on an Electrochemical Analyzer Model CHI830B, CHInstruments Inc., TX, USA, with a three electrode configuration and a

working volume of 3 mL. An Ag/AgCl electrode (Orion,Beverly, MA, USA) and a platinum plate electrode served as the reference and counter electrodes, respectively. All potentials given in this chapter are relative to the Ag/AgCl electrode. The working electrodes were modified graphite paste electrodes (GPE) and prepared using active paste of (i) PBNPs-$AgNP_1$, (ii) FcCOOH with $PdNP_5$ and (iii) FcCOOH with $PdNP_6$.

5B.2.2. Fabrication of modified graphite paste electrodes

PBNP/PBNP–$AgNP_1$ modified carbon paste electrode was made using electrode body (MF-3010) obtained from Bioanalytical Systems Inc. West Lafayette. The active paste having composition (w/w): PBNP/PBNP–$AgNP_1$ = 3%, graphite powder = 67% (w/w), Nujol oil = 30% (w/w) was mixed thoroughly and stored in stoppered glass vials at room temperature. The active paste was filled into the well of the electrode body and the surface was manually smoothed on clean butter paper.

The as synthesized $PdNP_5$ and $PdNP_6$ [as discussed in Chapter three-section 3.2.2.2 (Table 3.3)] were adsorbed on graphite powder. The graphite mixed PdNPs was prepared by dropping 100 μl PdNPs sol with 100 mg graphite powder (particle size1-2 μm) followed by ultrasonication at 20 kHz for 20 min. The mixtures were left to stand at 50^{o}C overnight for complete evaporation of solvent. The PdNPs adsorbed on graphite particles were calcinated at 500^{o}C under nitrogen atmosphere to eliminate the organic functionality. The resulting solid residues (containing $PdNP_5$ and $PdNP_6$ adsorbed on graphite powder) were thoroughly mixed with Fc-COOH in a grinder. The absence and the presence of PdNPs in the active paste resulted into the formation of modified carbon paste electrode (CPE) as: CPE/Fc-COOH, CPE/FcCOOH-$PdNP_5$ and CPE/Fc-COOH-$PdNP_6$ systems (as shown in Table 5B.1). The electrode body used for the construction of graphite paste electrode was obtained from Bioanalytical Systems [West Lafayette, IN (MF 2010)]. The well of electrode was filled with an active paste of composition as shown in Table 5B.1. The desired amounts of modifiers were thoroughly mixed with graphite powder (particle size 1-2 μm) in a blender followed by addition of Nujol oil. Finally, the paste surface was manually smoothed on a clean butter paper.

Table 5B.1. Composition of modified carbon paste electrodes

Systems	Fc-COOH (w/w %)	PdNPs adsorbed on graphite (w/w %)	Graphite (w/w %)	Nujol oil (w/w%)
Fc-COOH	1.5	-	68.5	30
Fc-COOH-PdNP$_5$	1.5	30	38.5	30
Fc-COOH-PdNP$_6$	1.5	30	38.5	30

5B.2.3. H_2O_2 sensing over PBNPs and its nanocomposite modified electrodes

An analysis of electrochemical interaction of H_2O_2 and electrode material was studied based on cyclic voltammetry and recorded between the potential ranges of-0.2 to 0.5 Vs^{-1} vs Ag/AgCl. The H_2O_2 sensing was conducted by holding the modified electrodes at desired potential vs. Ag/AgCl in 0.1 M phosphate buffer (pH 7.0) containing 0.5 M KCl.

5B.2.4. AA sensing over FcCOOH and PdNPs modified electrodes

The AA sensing was carried out through cyclic voltammetry and by amperometric measurements at desired potentials vs. Ag/AgCl in 0.1 M phosphate buffer containing 0.5 M KCl (pH 7.0) using FcCOOH, FcCOOH-PdNP$_5$ and FcCOOH-PdNP$_6$ modified electrodes. All measurements were performed at room temperature (25^{o}C). The cyclic voltammograms were recorded before and after the addition of AA at the scan rate of 0.01 Vs^{-1} between the potential ranges of 0.2 to 0.6 V vs. Ag/AgCl. Further, the amperometric (AMP) response was recorded over the modified electrodes to figure out the lowest detection limit and sensitivity. AMP experiments were performed in a three electrode assembly at 0.25 Vs^{-1} vs. Ag/AgCl in 0.1 M phosphate buffer (pH 7) containing 0.5 M KCl the background current was allowed to decay to a steady-state value followed by addition of varying concentrations of AA and new steady-state current was recorded.

5B.3. RESULTS

5B.3.1. Electrocatalytic reduction of H_2O_2 over PBNPs and PB-$AgNP_1$ modified electrode

5B.3.1.1. Electrochemical characterization

The electrochemical behavior of PBNP and its nanocomposite based modified electrode was conducted to verify the synthesis of same. Figure 5B.1. shows cyclic voltammogram of PBNP-$AgNP_1$ modified electrode recorded in 0.1 M KNO_3. Two reversible redox couples were observed for PBNP-$AgNP_1$ modified electrode between the potential ranges of -0.2 to 1.0 V vs.Ag/AgCl. Further, Figure 5B.2 (a) and (b) show the cyclic voltammogram of PBNPs and PBNP-$AgNP_1$ modified electrode between the potential ranges of -0.2 to 0.5 V vs. Ag/AgCl.

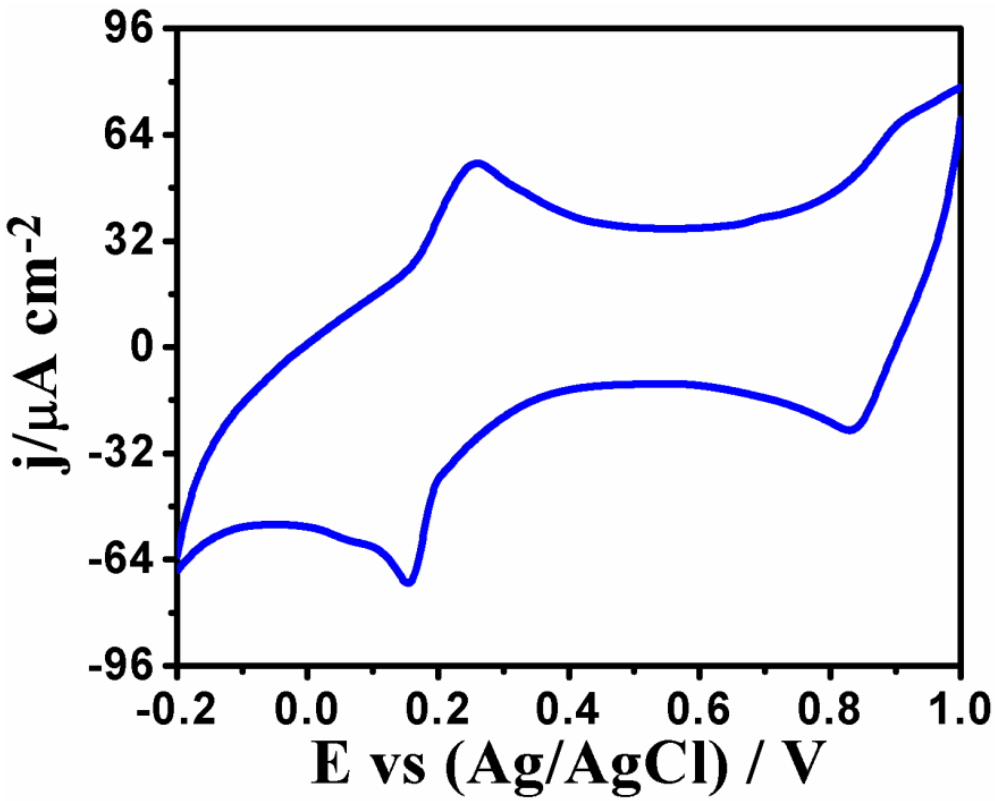

Figure 5B.1. The electrochemical behavior of nanocomposite PBNP-$AgNP_1$ between -0.2 to 1 V vs. Ag/AgCl in 0.1 M KNO_3 at scan rate of 0.01 V s^{-1}.

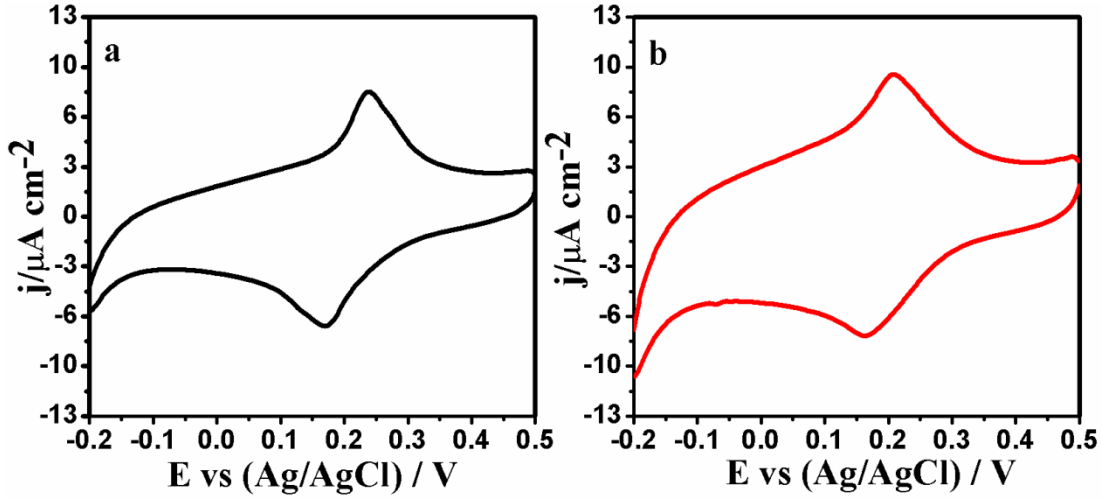

Figure 5B.2. Cyclic Voltammograms of PBNPs (a) and PBNP-$AgNP_1$ (b), between -0.2 to 0.5 V vs. Ag/AgCl in 0.1 M KNO_3 at scan rate of 0.01 V s^{-1}.

5B.3.1.2. Cyclic voltammetric response

The reduction of H_2O_2 was performed in a neutral condition, and herein phosphate buffer (0.1M, pH 7.0) was used as electrolyte solution. The cyclic voltammograms for the reduction of H_2O_2 over PBNPs and PBNP-$AgNP_1$ modified electrodes are shown in Figure 5B.3. As can be seen, the cathodic current recorded on the addition of an identical concentration of H_2O_2 in the case of PB-$AgNP_1$ (Figure 5B.3b) is relatively much higher than that in the case of PBNP system (Figure 5B.3a).

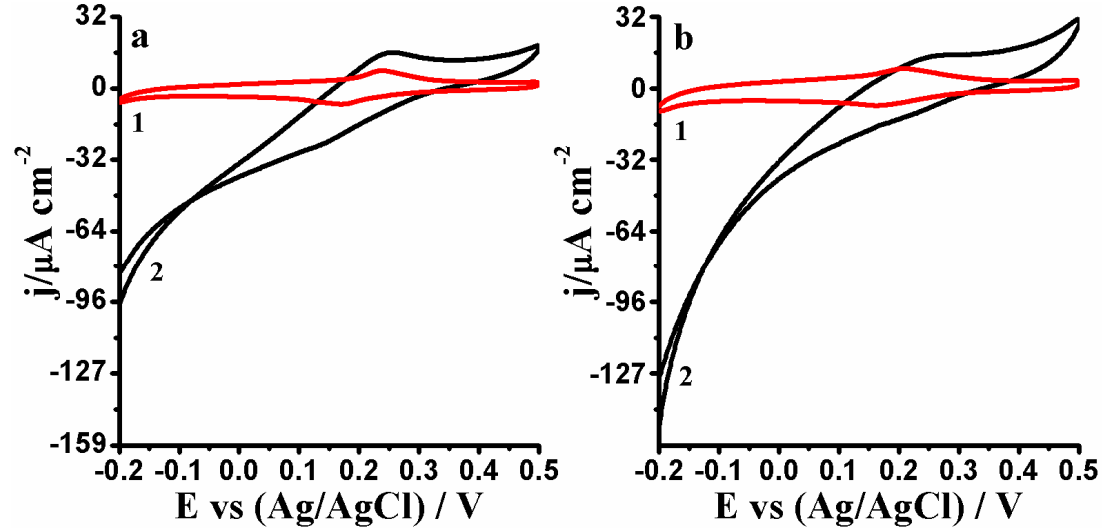

Figure 5B.3. Cyclic Voltammograms of PBNPs (a) and PBNP-$AgNP_1$ in absence (1) and the presence (2) of 5 mM H_2O_2 at the scan rate of 0.01 V s^{-1} in 0.1 M phosphate buffer (pH 7.0) containing 0.5 M KCl.

5B.3.2. Interaction of 3-APTMS with FcCOOH and role of PdNPs on the redox electrochemistry of FcCOOH

The important aspires of the present investigation is to understand the interaction of 3-APTMS and Ferrocene derivative. Such interaction may be affected by the polarity of the medium. Accordingly, the interaction of Fc-COOH and 3-APTMS has been studied in four different solvents i.e., (A) 0.1 M phosphate buffer (pH-7.0), (B) methanol, (C) acetonitrile and (D) toluene. The results on the variation of specific absorption of Fc-COOH in absence and the presence of 3-APTMS (5 mM) are shown in Figure 5B.4-5. The electrochemical behavior of Fc-COOH based on cyclic voltammetry in absence of 3-APTMS at different scan rates (0.01, 0.015, 0.035, 0.05, 0.07,0.1, 0.15, 0.25, 0.35 and 0.5) in 0.1 M phosphate buffer (pH- 7.0) as shown in Figure 5B.6 and in the presence of two concentrations of 3-APTMS (10 mM and 40 mM) at 0.01 Vs^{-1} in 0.1 M phosphate buffer (pH- 7.0) as shown in Figure 5B.7. To eliminate the presence of amino functionality from PdNPs (due to the interaction of 3-APTMS with FcCOOH) for understanding the role of palladium nanogeometry on the redox electrochemistry of FcCOOH, PdNPs adsorbed on graphite surface followed by calcination at 500^{o}C. Calcinated PdNPs incorporated into graphite paste electrode along with Fc-COOH to understand the redox behavior of the same in the presence of PdNPs. Figure 5B.8-10(a) shows the results based on cyclic voltammetry of Fc-COOH, Fc-COOH-$PdNP_5$ and Fc-COOH-$PdNP_6$ (as shown in Table 5B.1). The variation in the peak current as a function of scan rate has been shown in Figure 5B.8-10(b). The peak separation has been found to be 97 mV for FcCOOH, 92 mV for Fc-COOH-$PdNP_5$ and 69 mV for Fc-COOH-$PdNP_6$ under similar conditions that justify improvement in reversible redox behavior of Fc-COOH as a function of palladium nanogeometry.

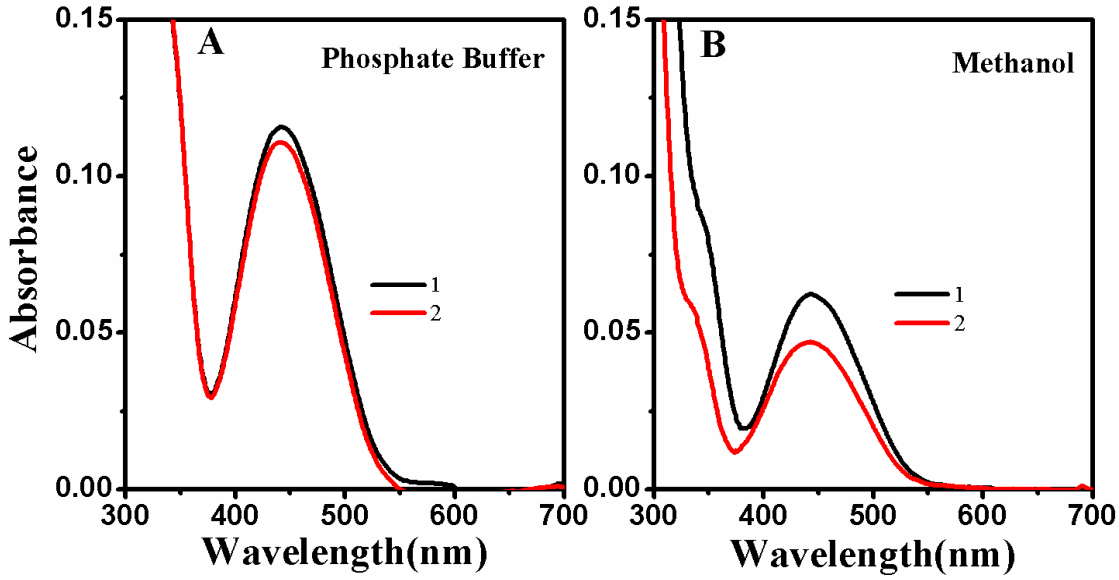

Figure. 5B.4. UV-Vis spectra showing the interaction between constant concentration of Fc-COOH (1) and 3-APTMS (2) in Phosphate Buffer (A) and Methanol (B).

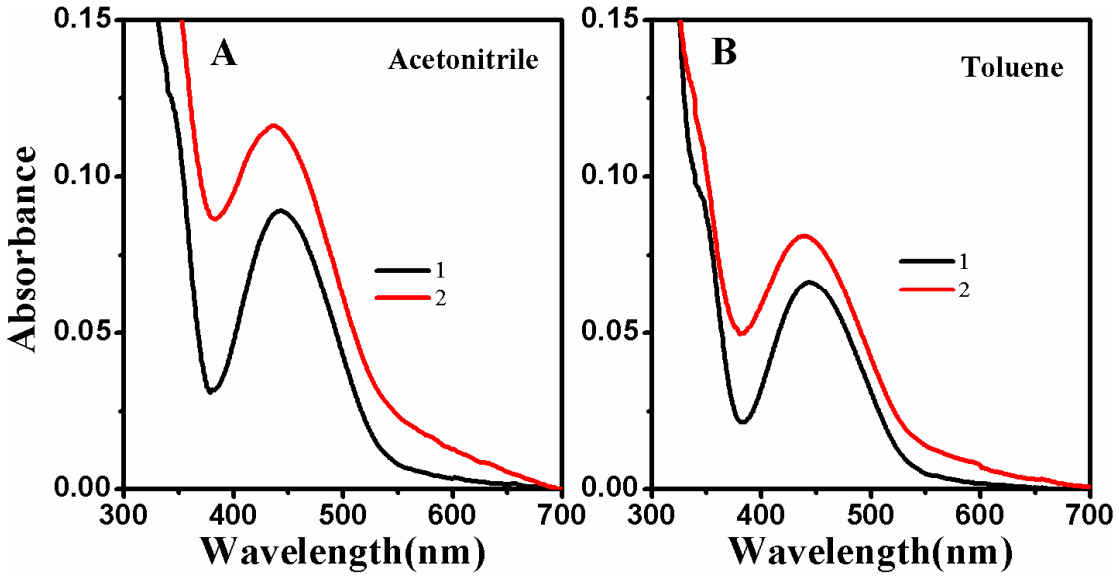

Figure. 5B.5. UV-Vis spectra showing the interaction between constant concentration of Fc-COOH (1) and 3-APTMS (2) in Acetonitrile (A) and Toluene (B).

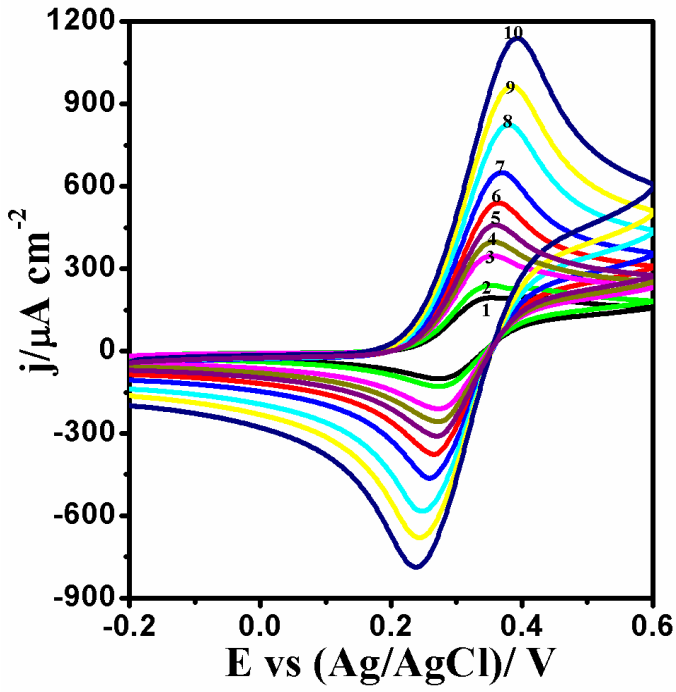

Figure. 5B.6. Cyclic voltammograms of Fc-COOH in 0.1 M Phosphate Buffer (pH-7.0) at various scan rates (Vs^{-1}); 1 = 0.01, 2 = 0.015, 3 = 0.035, 4 = 0.05, 5 = 0.07, 6 = 0.1, 7 = 0.15,8 = 0.25, 9 = 0.35 and 10 = 0.5;

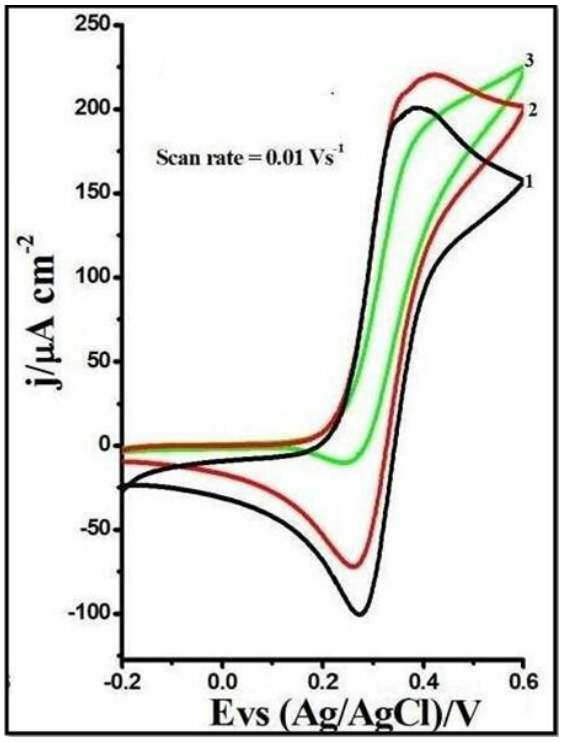

Figure. 5B.7. Cyclic voltammograms of FcCOOH in absence (1) and the presence of 10 mM 3-APTMS (2) and 40 mM 3-APTMS (3) at 0.01 Vs^{-1} in 0.1 M Phosphate Buffer (pH-7.0).

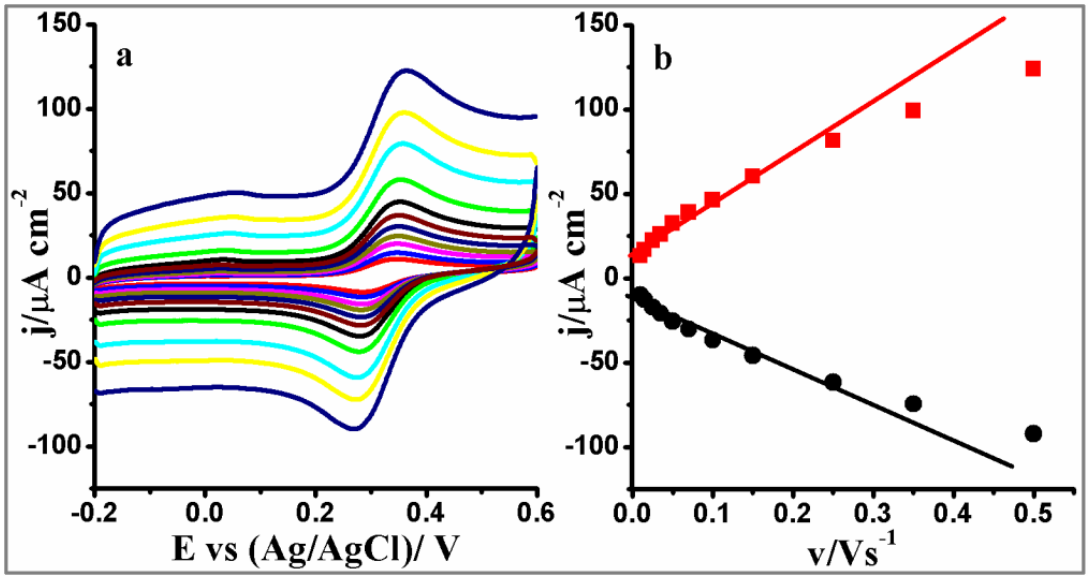

Figure. 5B.8. Cyclic voltammograms of Fc-COOH (a), in 0.1 M KCl at various scan rates between 0.01Vs^{-1} to 0.5 Vs^{-1}; (b) show corresponding plot of peak current density versus scan rate respectively.

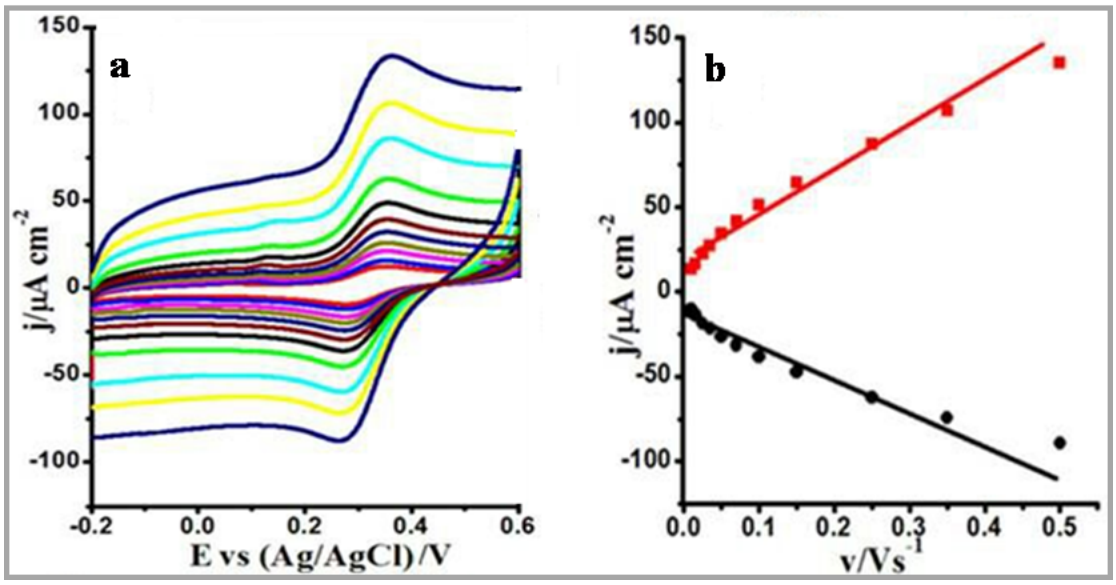

Figure. 5B.9. Cyclic voltammograms of Fc-COOH-$PdNP_1$ (a) in 0.1 M KCl at various scan rates between 0.01Vs^{-1} to 0.5 Vs^{-1}; (b) show corresponding plot of peak current density versus scan rate respectively.

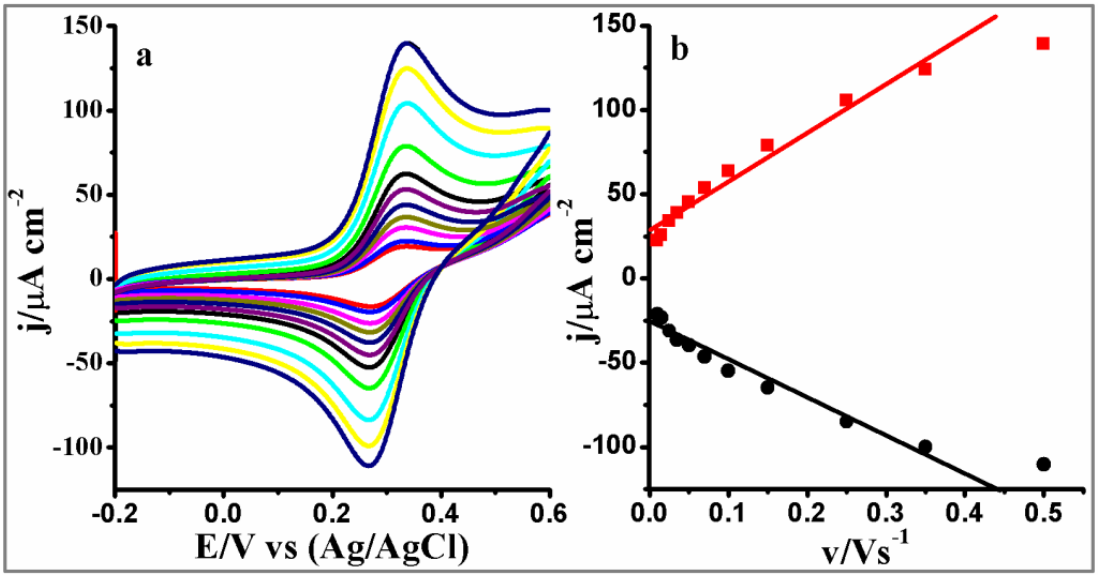

Figure. 5B.10. Cyclic voltammograms of Fc- COOH-$PdNP_2$ (a) in 0.1 M KCl at various scan rates between 0.01Vs^{-1} to 0.5 Vs^{-1}; (b) show corresponding plot of peak current density versus scan rate respectively.

5B.3.3. Electrochemical sensing of AA over FcCOOH and PdNPs modified electrode

5B.3.3.1. Cyclic voltammetric response

A need of neutral pH is necessary for the electrochemical oxidation of AA performed in an electrolyte solution. The cyclic voltammograms for the oxidation of ascorbic acid on FcCOOH, FcCOOH-$PdNP_5$ and FcCOOH-$PdNP_6$ are shown in Figure 5B.11 (a-c) respectively in absence (1) and the presence (2) of 1mM AA. As shown in Figure 5B.11(c), with the addition of 1mM AA, the FcCOOH-$PdNP_6$ modified system showed the higher oxidation current, compared to that of FcCOOH-$PdNP_5$ and FcCOOH modified system.

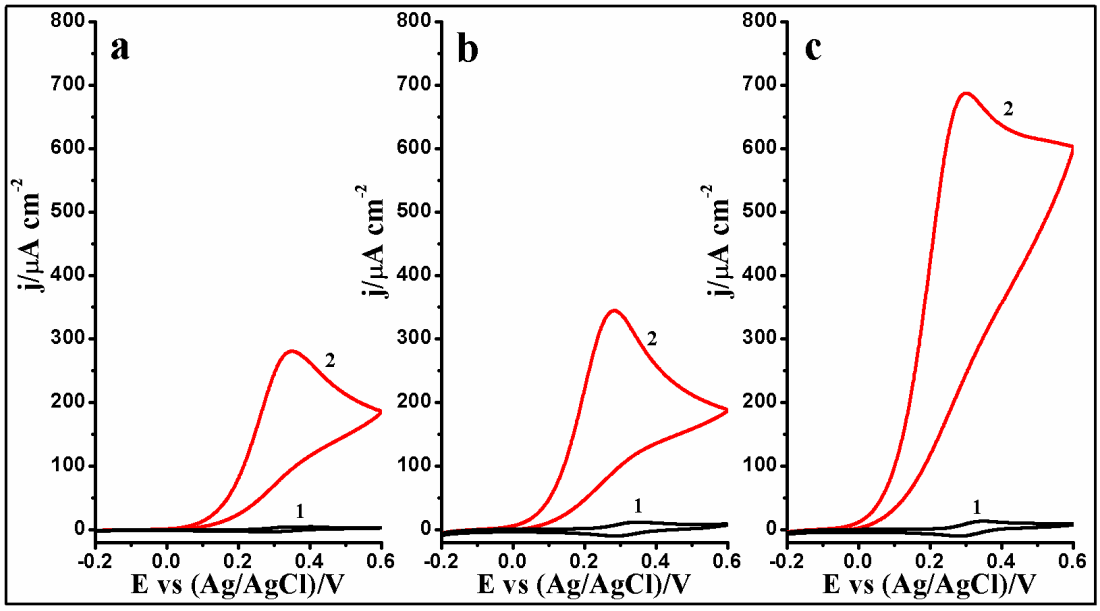

Figure.5B.11. Cyclic voltammograms of (a) Fc-COOH, (b) Fc-COOH-$PdNP_5$ and Fc-COOH-$PdNP_6$ systems in absence and the presence of 1 mM ascorbic acid at the scan rate of 0.01Vs^{-1} in 0.1 M phosphate buffer (pH 7.0) containing 0.5 M KCl.

5B.3.3.2. Amperometric response

The electrocatalytic performance of modified electrodes was also assessed by amperometric measurements under stirring condition. Amperometric measurements was performed by successively adding AA (10 nM to 5mM) to the continuously stirred solution with a working potential of 0.25 Vvs. Ag/ AgCl. Figure 5B.12 shows the amperometric responses of FcCOOH (a) FcCOOH-$PdNP_5$ (b) and FcCOOH-$PdNP_6$ (c) modified electrodes. It is clear from the figure that the FcCOOH-$PdNP_6$ modified electrodes showed higher response as compared to that of FcCOOH-$PdNP_5$ and FcCOOH modified electrode, again confirming the electrocatalytic behavior of the modifiers. The calibration curves for AA detection by amperometry were constructed as shown in the respective insets to Figure 5B.12 The sensitivity towards AA sensing was found to be 29.6, 60.4 and 79.6μA $mM^{-1}cm^{-2}$ for FcCOOH, FcCOOH-$PdNP_5$ and FcCOOH-$PdNP_6$ modified electrode respectively.

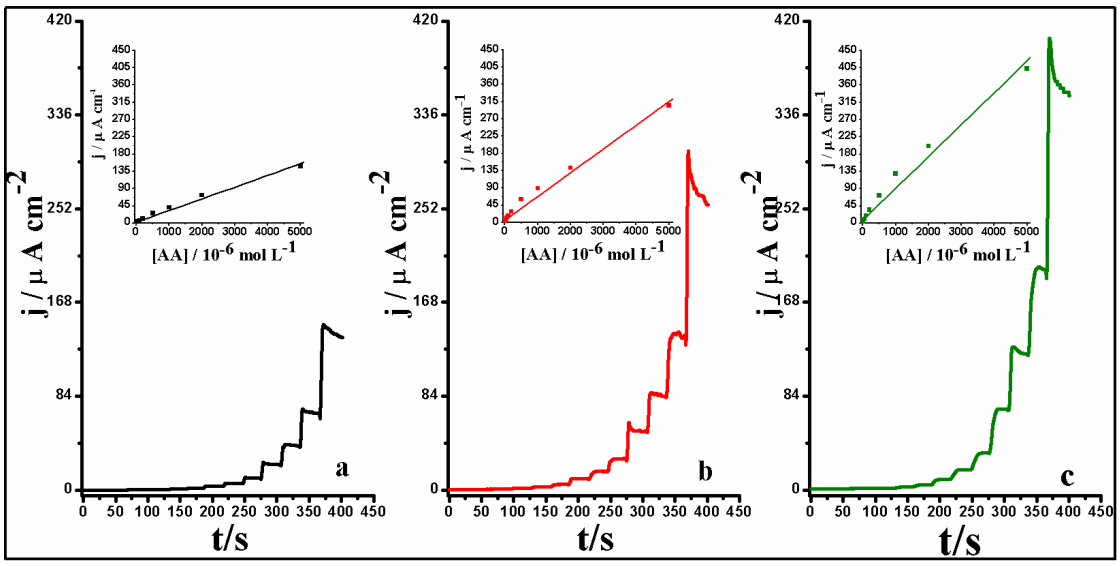

Figure. 5B.12. Amperometric response of Fc-COOH (a), Fc-COOH-$PdNP_5$ (b) and Fc-COOH-$PdNP_6$, modified electrodes in 0.1 M phosphate buffer (pH 7.0) containing 0.5 M KCl on the addition of varying concentrations of ascorbic acid at 250 mV vs Ag/AgCl.

5B.4. DISCUSSION

5B.4.1. Electrocatalytic probing of H_2O_2 over PBNPs and PBNP-$AgNP_1$ modified electrode

Apart from the homogeneous catalytic applications of the as synthesized nanocomposite, the finding on heterogeneous catalysis has also been explored. The PBNP–$AgNP_1$ nanocomposites (discussed in section 4.2.2.3) are used to make a chemically modified electrode for evaluating the electrocatalytic ability of the material. The presence of $AgNP_1$ with PBNP enable an improvement in the electrochemical behavior between -0.2 to 1 V vs. Ag/AgCl is shown in Figure 5B.1 revealing the significance of the chemically synthesized PBNP nanocomposite. Figure 5B.2 significantly increases the charge transport process as evidence from the peak separation, there is the peak separation of 20 mV as shown in Figure. 5B.2 (a) and (b) with respect to cathodic and anodic peak potential separation.

The electrocatalytic behavior of the PBNP–$AgNP_1$ nanocomposite has been examined for the reduction of H_2O_2 and compared to H_2O_2 reduction recorded on an unmodified PBNP-modified electrode, as shown in Figure 5B.3. H_2O_2 undergoes both

oxidation and reduction. The direct oxidation of H_2O_2 involves a large overvoltage whereas direct reduction of H_2O_2 starts at 0 V vs. Ag/AgCl and the dynamics of the reduction increases with an increase in cathodic potential [Pandey *et al*., (2001d)]. Catalytic reduction, as shown in Figure 5B.3, start close to the redox potential of PBNP and subsequently follow a similar trend, as observed in direct reduction. The use of Horseradish peroxidase (HRP) also facilitates the reduction of H_2O_2 at a slightly anodic potential and the dynamics increase with an increase of operating potential in cathodic direction [Pandey *et al*., (2001d)] similar to that as recorded in Figure 5B.3.

The results based on voltammetry for Figure 5B.3 (a) PBNP and (b) PBNP–$AgNP_1$ systems in absence and the presence of 5 mM H_2O_2 confirm the improved catalytic behavior of the PBNP–$AgNP_1$ electrode system. The finding confirms the enhanced electrocatalytic activity of nanocomposite compared to pure PBNP for H_2O_2 analysis. Again, the modified electrode is a suitable material for electrochemical probing of many oxidase catalyzed reaction coupledin a flow injection system, presenting the wider application of nanocomposite modified electrodes for the efficient detection of H_2O_2 generated in an enzymatic packed bedreactor [Pandey and Weetall., (1995)].

5B.4.2. Effect of 3-APTMS and PdNPs on the redox electrochemistry of FcCOOH

In order to understand, the interaction of 3-APTMS and Ferrocene derivative while encapsulating the former within ormosil network useful in Bioelectrocatalysis, the results reported earlier [Pandey *et al*., (1999e)] demonstrated sluggish reversible electrochemical behavior of Fc-COOH within such nanostructured network directing for evaluating the specific interaction between Fc-COOH and 3-APTMS. Such interaction affected by the polarity of the medium and has been studied in four different solvents. And the results based on these lines are shown in Figure 5B.4 and 5B.5 justify that the absorbance of Fc-COOH decreases in the presence of 3-APTMS in polar solvents (Figure 5B.4) and increases in non-polar solvents (Figure 5B.5)

under similar conditions. The finding clearly demonstrates the role of polarity on exploiting the functional activity of Fc-COOH in the presence of 3-APTMS.

We subsequently studied the electrochemical behavior of Fc-COOH based on cyclic voltammetry with the 3-APTMS in 0.1 M phosphate buffer (pH 7.0). The results based on electrochemical behavior of Fc-COOH in absence and the presence of 3-APTMS as shown in Figure 5B.6 and 5B.7. There is a slight increase in anodic current and decrease in cathodic current on the addition of 3-APTMS revealing mediated oxidation of 3-APTMS by Fc-COOH (Figure 5B.7). An increase in 3-APTMS concentration (Figure 5B.7, curve-3) again support significant decrease in cathodic current whereas anodic current is converted into a plateau and do not support efficient ferrocene mediated oxidation of 3-APTMS in phosphate buffer. Accordingly, efficient mediated electrochemical oxidation of propylamine (PrA), diethylamine (DEA), pyrrolidine (Pyr), and triethylamine (TEA) by ferrocene (Fc) in acetonitrile was recorded justifying concentration dependent increase in anodic current followed by decrease in cathodic current as expected for mediated electrocatalysis reported earlier by Bond *et al.* [Torriero *et al.*, (2013)]. The results on the interaction of 3-APTMS and Fc-COOH based on spectroscopy (Figure 5B.4 and 5B.5) and electrochemistry ((Figure 5B.4 and 5B.5) clearly justify the interaction of amino-residue with ferrocene moiety reflecting decrease in charge transport in the presence of 3-APTMS in polar medium.

Earlier report [Pandey *et al.*, (2001c)] justify that presence of palladium does not retard the redox electrochemical activity of the Fc-COOH and instead promote faster electron exchange from the same. However, the findings based on UV-Vis spectroscopy (Figure 5B.4 and 5B.5) and electrochemical measurements (Figure 5B.4 and 5B.5) justify the interaction of 3-APTMS with ferrocene derivatives and direct to review the role of 3-APTMS during electron-exchange process in the presence of palladium nanoparticles in homogeneous medium. The findings on the role of 3-APTMS in the presence of metal ions [Pandey and Chauhan., (2012); Pandey and Pandey., (2014c)] reveals the reducing ability of the same and further 3-APTMS serve as potential electron donor in the presence of other similar reagents like GPTMS/THF-HPO/Cyclohexanone. Such activity of

3-APTMS enables an increase in electron density around metal ions leading to the reduction of the same in the presence of charge transfer sites. Accordingly, the presence of 3-APTMS may promote partial charge transfer to cyclopentadienyl sandwiched iron that ultimately retards the subsequent electrochemical reduction of the same in polar medium (Figure 5B.7). In addition to that the hydrophilic character of 3-APTMS might be playing pivotal role suggesting ferrocene mediated oxidation of PdNPs into palladium ion in homogeneous medium and required detailed investigation. When such redox species is replaced by potassium ferricyanide having coordinated groups in d-shell, the presence of 3-APTMS does not affect the redox activity since potassium ferrocyanide and potassium ferricyanide are potential electroactive species and show reversible redox behavior in both forms. Accordingly, the presence of 3-APTMS while using palladium linked GPTMS did not affect the electrochemical behavior of ormosil-encapsulated potassium ferricyanide [Pandey *et al*., (2003a)]. These findings suggest to eliminate the presence of amino functionality from PdNPs for the role of palladium nanogeometry on the redox electrochemistry of Fc-COOH and directed to calcinate the same at 500^{o}C for meeting such requirement. Accordingly, we calcinated 3-APTMS stabilized $PdNP_5$ and $PdNP_6$ at 500^{o}C after careful adsorption of nanoparticles suspension on graphite powder. These calcinated PdNPs incorporated into graphite paste electrode along with Fc-COOH to understand the redox behavior of the same in the presence of PdNPs since an increase in the distance between PdNPs adsorbed on graphite particles and ferrocene may lead to poor electrochemical interaction. The results on the variation of the redox behavior of Fc-COOH in the presence of calcined $PdNP_5$ and $PdNP_6$ within graphite paste electrode as shown in Figure 5B.8-10(a). The finding reveals reversible redox electrochemistry of Fc-COOH and justifies the need for eliminating the amino-functionality to understand the effect of palladium on electrochemical behavior of the same. And the results in the peak current as a function of scan rate shows in the Figure 5B.8-10(b). The gradual improvement in linear relation of peak current versus scan rate demonstrates the effect of PdNPs of variable nanogeometry on the redox electrochemistry of Fc-COOH. The peak separation has been found to be 97 mV for Fc-COOH, 92

mV for Fc-COOH-$PdNP_5$ and 69 mV for Fc-COOH-$PdNP_6$ under similar conditions that justify improvement in reversible redox behavior of Fc-COOH as a function of palladium nanogeometry. It is also to be noted that nanogeometry of $PdNP_5$ and $PdNP_6$ remains analogous after calcinations. It is again important to review such variation in electrochemical behavior of Fc-COOH as a function of palladium nanogeometry since PdNPs were adsorbed on graphite particle and subsequently confined within graphite paste together Fc-COOH. The electrochemistry of surface confined mediator within reaction zone is the function of electron hopping sites that subsequently control the charge transport within reaction zone. An increase in palladium nanogeometry relatively increases the hopping sites as reported earlier [Pandey et al., (2003a)]. Accordingly, the reversible electrochemical behavior of Fc-COOH tends to be improved in the presence of $PdNP_7$. Such finding also reflect role of distance between hopping sites and redox centres of the mediators on the charge transport that may again be facilitated on decreasing the same as reported earlier [Degani and Heller., (1987); Pandey *et al*., (1991)].

5B.4.3. Electrochemical sensing of AA: Role of different sizes of Palladium nanoparticles

The PdNPs modified graphite paste electrodes were used to examine the electrocatalytic activity of these materials on the oxidation of ascorbic acid (AA). Figure 5B.11 shows the cyclic voltammogram of (a) Fc-COOH, (b) Fc-COOH-$PdNP_5$ and (c) Fc-COOH-$PdNP_6$ respectively in absence and presence of 1 mM AA. The results clearly demonstrate an increase in electrocatalysis as a function of nanogeometry of PdNPs (Figure 5B.11a-c). Such finding is further supported from the amperometric responses of these electrodes recorded in 0.1 M phosphate buffer (pH 7.0) at 250 mV vs. Ag/AgCl. The varying concentrations of AA were added at steady-state response of the sensor followed by recording another steady state value. The data are recorded in Figure 5B.12 for these three systems. The inset to Figure 5B.12 a, b and c shows the corresponding calibration curves for AA analysis. The sensitivity calculated for these three systems were found to be 29.6 for Fc-COOH, 60.4 for Fc-COOH-$PdNP_5$ and 79.6 $\mu A\ mM^{-1}cm^{-2}$ for Fc-COOH-$PdNP_6$ and confirmed the role of

nanogeometry on electrocatalysis. The results reveals the following information: (1) gradual amplification in sensing response from system-1 (Fc-COOH) to system-3 (Fc-COOH-$PdNP_6$), (2) better electrocatalytic behavior of Fc-COOH-$PdNP_6$ as compared to that of Fc-COOH-$PdNP_5$ and (3) significant improvement on the catalytic behavior of Fc-COOH in the presence of palladium nanoparticles as a function of their nanogeometry.

Reproducibility and Stability of the modified electrode

The reproducibility of the present modified electrodes has been investigated by examining the amperometric responses in 0.1 M phosphate buffer (pH 7.0) containing 5 mM AA. The relative standard deviation (RSD) is found to be 3.4% for 6 successive measurements. The storage stability of the Fc-COOH-$PdNP_6$ modified electrode was also investigated by monitoring its response to 5 mM AA, and it remained about 95% of its original sensitivity after two week. These findings indicate admirable reproducible and stable electrochemical behavior of the Fc-COOH-PdNPs during AA detection.

5B.5. CONCLUSION

The studies conducted in the present section deals with the potential application of above synthesized nanomaterials. The finding revealed the following: (i) an efficient H_2O_2 sensor has been fabricated based on application of PBNPs and its nanocomposite with $AgNP_1$; (ii) the PBNP-$AgNP_1$ nanocomposite significantly increased the sensitivity of H_2O_2 analysis as compared to that of PBNPs, reflecting the contribution of $AgNP_1$ in electrocatalysis; (iii) 3-APTMS is found to influence the redox electrochemical behavior of Fc-COOH in polar medium; (iv) PdNPs synthesized through 3-APTMS and THF-HPO gradually improves the electrochemistry of Fc-COOH as a function of nanogeometry and usability in synthesizing the electrochemical sensor design; (v) These findings indicate admirable reproducible and stable electrochemical behavior of the Fc-COOH-PdNPs during AA detection.